A novel high pressure column flow reactor for experimental studies of CO₂ mineral storage

I. Galeczka [a,*], D. Wolff-Boenisch [a], T. Jonsson [a], B. Sigfusson [b], A. Stefansson [a], S.R. Gislason [a]

[a] Institute of Earth Sciences, University of Iceland, Sturlugata 7, 101 Reykjavik, Iceland
[b] Reykjavik Energy, Baejarhals 1, 110 Reykjavik, Iceland

ARTICLE INFO

ABSTRACT

The objective of this study was to design, build, and test a large scale laboratory high pressure column flow reactor (HPCFR) enabling experimental work on water–rock interactions in the presence of dissolved gases, demonstrated here by CO₂. The HPCFR allows sampling of a pressurized gas charged liquid along the flow path within a 2.3 m long Ti column filled with either rock, mineral, and/or glass particles. In this study, a carbonated aqueous solution (1.2 M $CO_{2(aq)}$) and basaltic glass grains was used. Given the pressure and temperature rating (up to 10 MPa at 90 °C) of the HPCFR, it can also be used with different gas and/or gas mixtures, as well as for supercritical fluid applications. The scale of the HPCFR, the possibility of sampling a reactive fluid at discrete spatial intervals under pressure, and the possibility of monitoring the evolution of the dissolved inorganic carbon and pH *in situ* all render the HPCFR unique in comparison with other columns constructed for studies of water–rock interactions. We hope that this novel experimental device will aid in closing the gap between bench scale reactor experiments used to generate kinetic data inserted into reactive transport models and field observations related to geological carbon sequestration. A detailed description and testing of the HPCFR is presented together with first geochemical results from a mixed H₂O–CO₂ injection into a basalt slurry whose solute concentration distribution in the HPCFR was successfully modelled with the PHREEQC geochemical computer code.

© 2012 Elsevier Ltd. All rights reserved.

1. Introduction

Mineral sequestration is the final product of geological carbon storage which provides long-term stability for captured, industrial CO₂. In fact, mineral storage mimics the natural processes of weathering of primary silicates and magmatic CO₂ flux into groundwater systems in silicate rocks (Flaathen et al., 2009). Atmospheric carbon can be transformed into carbonate minerals either *ex situ*, as part of an industrial process, or *in situ*, by injection into geological formations where the elements required for carbonate–mineral formation are present (Oelkers et al., 2008). The relative amount and rate of CO₂ fixation depend on the rock type (Wolff-Boenisch et al., 2006), injection methods and temperature. Investigation of basaltic and ultramafic rocks (Gislason et al., 1993; McGrail et al., 2006; Matter et al., 2007; Kelemen and Matter, 2008; Garg and Shukla, 2009; Prigiobbe et al., 2009; Schaef and McGrail, 2009; Wolff-Boenisch et al., 2011; Gysi and Stefánsson, 2012a) demonstrate their high capacity for *in situ* carbonatization. The CarbFix CO₂ sequestration pilot project in Iceland (Gislason et al., 2010; Aradóttir et al., 2012) has been established to investigate *in situ* the potential for mineral carbon storage in basalt. The conceptual model of the CO₂ fixation into basaltic rocks indicates that CO₂ saturated waters will enhance basalt dissolution due to their low pH, releasing divalent metals into solution. As a result of proton consumption by basalt dissolution, pH will increase followed by carbonate ((Ca,Mg,Fe)CO₃) precipitation (McGrail et al., 2006; Oelkers et al., 2008; Gislason et al., 2010; Aradóttir et al., 2012).

There have been numerous experimental studies investigating H₂O–CO₂–basalt interaction. Many of them were focused on basalt dissolution rate measurements (Gislason and Eugster, 1987; Gislason et al., 1993; Schaef and McGrail, 2009; Gudbrandsson et al., 2011; Wolff-Boenisch et al., 2011); others were geared towards the effects of basalt carbonatization (Stockmann et al., 2011), whereas a third group combined basaltic dissolution and re-precipitation processes under CO₂ pressure (Gysi and Stefánsson, 2012a,c). Even though most of these experiments were carried out in small reactors of hundreds of millilitre volumes filled with few grams of rock, results of these experiments confirm the efficiency of basalt dissolution leading to its carbonatization under CO₂ pressure. The outcome of these experimental studies was a motivation to go a step further and bridge laboratory experiments and field observations by designing and constructing a large scale (2.3 m) high pressure column flow reactor (HPCFR; alternatively called 'plug' or 'plug flow reactor' in the literature) which will combine fluid flow through porous media, dissolution and precipitation of minerals and glasses under variable CO₂ partial or gas mixture pressure, fluid composition, and temperature.

* Corresponding author. Tel.: +354 849 0628; fax: +354 562 9767.
E-mail address: img3@hi.is (I. Galeczka).

A HPCFR is a cylindrical container filled with solid material where fluids are pumped through. At its inlet, dissolution reactions are predominant but over time and space, as the concentrations of reagents decrease and the concentrations of products increase along the reaction path, precipitation becomes more important. Despite the advantage of high chemical reaction rates, few laboratory studies have been published on percolation of CO_2-rich solutions through columns (Bateman et al., 2005, 2011; Andreani et al., 2009; Luquot and Gouze, 2009; Yi et al., 2011; Munz et al., 2012). The fact that not many column studies on pressurized water–rock interaction exist may be because large scale laboratory HPCFR of several metres are more difficult to design and maintain than their smaller batch and mixed-flow analogs, especially under elevated gas or hydraulic pressure. In a pressurized system, each connection (fittings, valves) inserted into the system poses a potential problem. Sampling procedure for a liquid under pressure is very challenging and special conditions have to be provided to obtain pH and CO_2 concentrations of a sample *in situ*, that is, under experimental conditions. The following experimental set-up makes it possible to monitor pH, Eh and chemical composition of the fluid along the flow path within the column, and also variations over time. Furthermore, a spatial study of the solid chemistry along the flow path can be performed due to divisions of the column into compartments (see Section 3.1 and Fig. 1). This spatial and temporal resolution at a higher scale is the most fundamental difference to common practice batch and flow-through reactor experiments. Because of this it can be used to "test" the performance of reactive transport models like PHREEQC (Parkhurst and Appelo, 1999) and

TOUGHREACT (Xu et al., 2006, 2011). The latter was used to predict the reactive transport properties of CO_2 injection into basaltic rocks at the CarbFix site in Iceland (Aradóttir et al., 2012). Information obtained during column experiments will improve our understanding of the kinetics of basalt dissolution and solid replacement reactions under CO_2 sequestration conditions. Future characterization and quantification of secondary minerals (carbonates, clays) will yield molar volume and porosity changes as a function of time and distance along the flow path. Data provided from the experiment will be used in reactive transport models to elucidate the advance of reaction fronts, forecast porosity changes and estimate more accurately the amount of sequestered CO_2.

This study discusses in detail the HPCFR design and technical issues such that it may serve as a guide for future experimental studies of supercritical fluid/gas–water–rock interactions. The HPCFR was tested with CO_2 charged waters (1.2 M $CO_{2(aq)}$) and basaltic glass as reactive material but in fact all kinds of material and different gases or gas mixtures can be used. The first results from the column, mimicking CO_2 injection into glassy basalt at $\sim$4 MPa pCO_2 and 22 °C are presented.

2. Material

The filling material for the column is basaltic glass originating from the Stapafell Mountain located in SW Iceland. This material has been utilized in previous studies on glass dissolution kinetics (Oelkers and Gislason, 2001; Gislason and Oelkers, 2003; Stockmann et al., 2011; Wolff-Boenisch
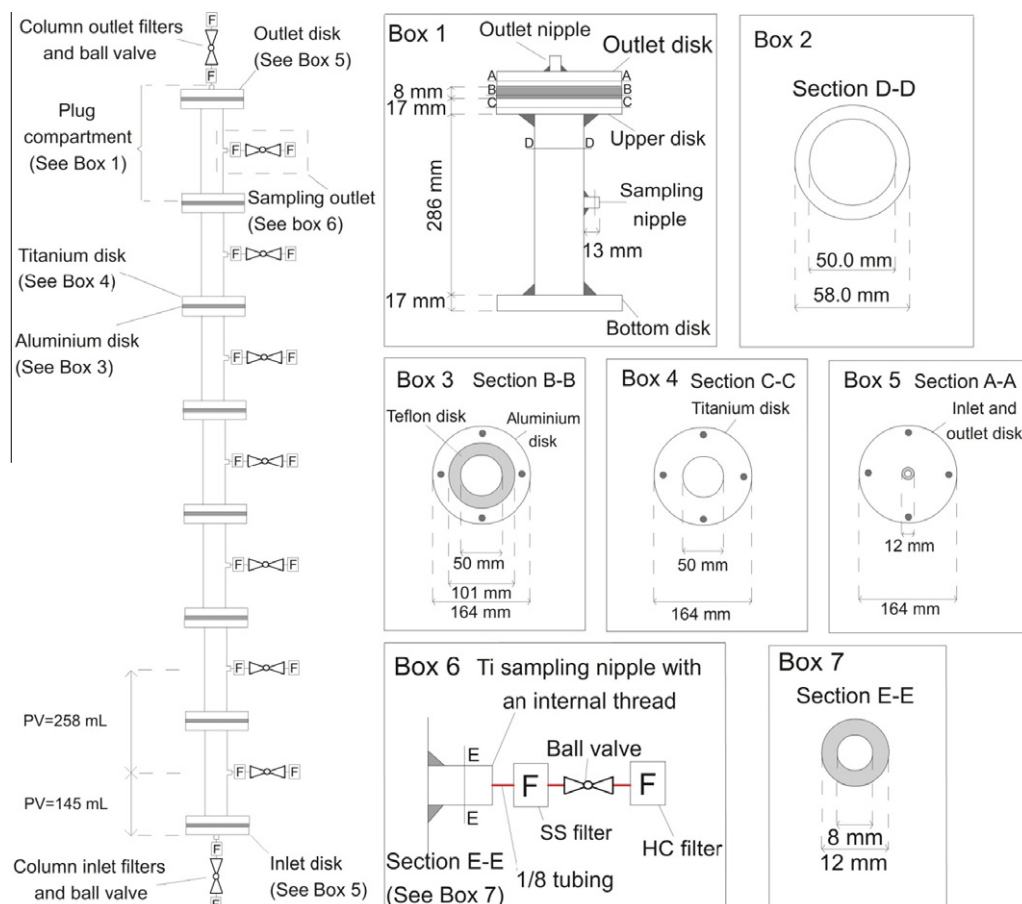

Fig. 1. Overall drawing of the 2.34 m long column is shown on the far left, with details displayed in Boxes 1–7. Box 1 illustrates the column outlet compartment in frontal view. Boxes 2–5 depict, in top view, the dimensions of the various compartments presented in Box 1. Box 6 describes the sampling outlet of each compartment and Box 7 displays, in top view, the dimensions of the sampling nipple. 'PV' in the overall drawing on the left refers to the pore volume in the compartments after filling the reactor with the solid material. Total length of the column is 2.34 m, the volume is 4.6 L, and the pore volume is assumed to be 40% ($\sim$1.84 L).

et al., 2011) and its chemical composition is consistent with $Si_{1.0}Ti_{0.024}Al_{0.355}Fe_{0.207}Mg_{0.276}Ca_{0.265}Na_{0.073}K_{0.007}O_{3.381}$. The 45–100 μm particle size fraction was dry sieved and washed by repeated gravitational settling to remove ultrafine particles. The total mass of glass inside the column is 8.3 kg, the corresponding specific BET surface area equals 22,000 cm^2/g, while the total surface area amounts to 182,160,000 cm^2. The total mass of aqueous solution is estimated as 1.84 L assuming 40% porosity, yielding a surface area to solution volume ratio of ~10^5 cm^{-1}.

3. Experimental set-up

Liquid CO_2 is mixed with degassed deionized (DI) water and pumped through a 2.3 m long Ti column filled with basaltic glass powder. Dissolution and precipitation reactions take place inside the HPCFR and reaction progress is monitored via solute sampling together with pH and DIC (Dissolved Inorganic Carbon) determinations in different compartments at increasing distances from the column inlet. The residence time of the fluid (total volume of the aqueous solution inside the column divided by the sum of the individual pump flow rates) can vary from a few to tens of hours. Total pressure is set at 8 MPa to keep the CO_2 in the liquid phase (see Section 3.2); however this value can differ depending on the temperature, gas or gas mixtures used in experiment.

The description of the HPCRF and its functioning can be divided into four subsections. The first section focuses on the column itself, containing the basalt slurry where chemical reactions between solid material and inlet solution occur. The second section depicts the reactive inlet solution supply. The third section covers the combination of electrical stream selectors and valves, gas expander, and back pressure regulators which enable sampling the outlet solution under physical and chemical conditions that prevail in the column, without alteration. The fourth section defines the in-line determination of the parameters pH, Eh and CO_2.

The CO_2 saturated inlet solution has a low pH and is, therefore, corrosive. Using materials with superior resistance to corrosive attack prevents changing solution chemistry caused by reaction between the corrosive liquid and plug material. Therefore, nearly the entire reactor is made either of Ti, Hastelloy® C-276 (HC), or PEEK (Polyether ether ketone). Titanium alloys can be used up to 600 °C and pressure up to 180 MPa depending on the type and thickness of the alloy and the temperature. It also has a high corrosion resistance to brines, seawater, and high ionic strength aqueous chloride solutions. Titanium performance, however, can be limited in strong, highly reducing acid media such as moderately or highly concentrated solutions of HCl, HBr, H_2SO_4, H_3PO_4 and in HF solutions as the temperature increases. Likewise, Hastelloy® C-276 shows outstanding performance in a variety of industrial applications. It can be used up to 1000 °C and is corrosion resistant to hot contaminated media (organic and inorganic), a variety of organic acids, seawater and brines, S compounds and Cl^- ions. In the HPCFR set-up, there are some exceptions where 316 stainless steel (SS) parts which are less corrosion resistant in acidic environments (especially at temperatures >66 °C) were used. It is assumed that in these instances contact time between SS and acidic fluid is so short that corrosion will have a negligible influence on the solute chemistry and material behavior. Furthermore, in the CO_2–basalt system the pH will not remain acid permanently but will evolve towards a circum-neutral range with progressing chemical reactions along the flow path, resulting in less corrosion.

3.1. The plug

The Ti column measures 234 × 5.8 × 5.0 cm, [length × outer diam. (OD) × inner diam. (ID)] and holds a total volume of ~4.6 L

(Fig. 1). It is anticipated that in the lower part of the column, dissolution of primary basaltic material will be the dominant process whereas precipitation of secondary phases will prevail in the upper part. Thus, the column was divided into seven compartments to allow a better spatial resolution of the reaction progress (Fig. 1, Box 1). Titanium disks of 16.4 × 5.0 cm [OD × ID] size were welded to each pipe compartment to create a flange (Fig. 1, Box 4). Additionally, two Ti inlet and outlet disks with 1/8″ compression fittings were added (Fig. 1, Box 5). All compartments together with upper and bottom flanges were properly screwed together with Teflon disks and O-ring rubbers wedged in between to assure a leak-free system up to a minimum of 10 MPa total pressure (Fig. 1, Box 3). Teflon is resistant to high temperatures up to 260 °C and to many chemicals (ozone, chlorine, acetic acid, ammonia, sulfuric acid and hydrochloric acid). The only substance which could affect Teflon performance and potentially create leakage in the pressurized column is molten alkali metals and highly reactive fluorinating agents. The small ID of the column compared to its length provides long flow paths for the reactive solution.

The inlet is placed at the bottom of the vertically aligned column to spread the percolating fluid perpendicular to the flow axis and to avoid preferential flow paths via gravitational resistance and lateral spread. The column has one main outlet at the top and seven lateral sampling outlets, one in each segment (Fig. 1, Box 6). Solution sampling from seven compartments enables the determination of changes in concentration of individual elements including DIC as well as pH and redox conditions along the flow path within the column. At all outlets of the column 1/8″ compression fittings are connected to 1/8″ SS 60 μm (Swagelok®) and HC 10 μm filters (VICI®) to avoid glass particles from the column entering and potentially clogging the sampling valves (see also Section 3.3 and Fig. 1). A SS ball valve (Swagelok®) is placed between both filters. The HC filters clogged during the initial testing of the plug. These filters consist of frits with a small cross sectional area and thus tended to clog very rapidly. It was decided to insert SS filters (Swagelok®) which contain frits with much larger cross sectional areas before the HC filters (Fig. 1, Box 6). Ball valves between the filters facilitate the replacement of the HC filter frits in case of clogging by closing the column outlet valves (Box 6 in Fig. 1). The column inlet and outlet filters (Fig. 1 far left) are connected to Ti 1/8″ needle valves (Collins Instrument) because contact with the reactive fluid is quasi permanent. In contrast, the seven sampling outlets are connected to SS 1/8″ ball valves (Swagelok®) as the short contact time between fluid and sampling valves is considered to exert a negligible influence on the solution chemistry. In order to avoid detrimental temperature swings in the laboratory, the column is wrapped with a heating tape (HTS/Amptec) maintained at ambient temperature (22 °C). This heating tape also circumvents the development of temperature gradients inside the column and enables promotion of chemical reactions when used at higher system temperatures (max. 90 °C given the pressure rating for the Ti plug thickness of 0.4 cm) which was, however, not explored in this study. The total pore volume of the water inside the column is estimated as ~1.84 L assuming a porosity of 40%. This pore volume is divided into eight sections where the beginning of the section starts with the previous sampling outlet and ends with the following one. The pore volume ('PV' in Fig. 1) of the bottom and the top section of the column is 145 mL, respectively whereas the pore volumes between two adjacent sampling outlets equal 258 mL.

3.2. Reactive fluid supply

The liquid CO_2 cylinder is placed on a scale and its status monitored through mass loss as shown in Fig. 2a. The cylinder is connected to a supercritical fluid pump (Supercritical Fluid

Technologies) through SS 1/8″ tubing. To provide sufficient head space delivery pressure from the CO_2 cylinder to the pump (>5.2 MPa), the distance between both has to be short and the gas cylinder kept at constant room temperature. It is recommended to use a tank heater (Power Modules, Inc.) to increase the head space cylinder pressure if low flow rates are used. To ensure thorough and complete mixing and dissolution of CO_2 in water ($CO_{2(aq)}$), liquid CO_2 ($CO_{2(l)}$) was given preference over a gaseous CO_2 ($CO_{2(g)}$) source because the solubilization kinetics of $CO_{2(l)}$ are fast (Bortoluzzi et al., 2011). The downside of $CO_{2(l)}$ is that the system pressure has to be maintained at or above 7.1 MPa, necessary to keep CO_2 liquid at room temperature. This calls for the installation of a high pressure corrosion resistant mixing device, ideally with sufficient volume to enable longer residence times for H_2O–CO_2 mixing. This requirement was solved by a flow-through Ti reactor like the ones routinely employed in mineral dissolution studies (Wolff-Boenisch et al., 2011). The liquid $CO_{2(l)}$ and DI water enter separately through the same dip tube and are thoroughly mixed by a magnetic stirrer before exiting through a 2 μm outlet reactor Ti filter (Fig. 2a). This 'mixing chamber' has the additional advantage of adjusting and controlling the mixing temperature. It should be pointed out that there are alternative ways to achieve thorough mixing (Luquot and Gouze, 2009) by coiled tubing in a water jacket (mixing loop) to dissolve $CO_{2(l)}$
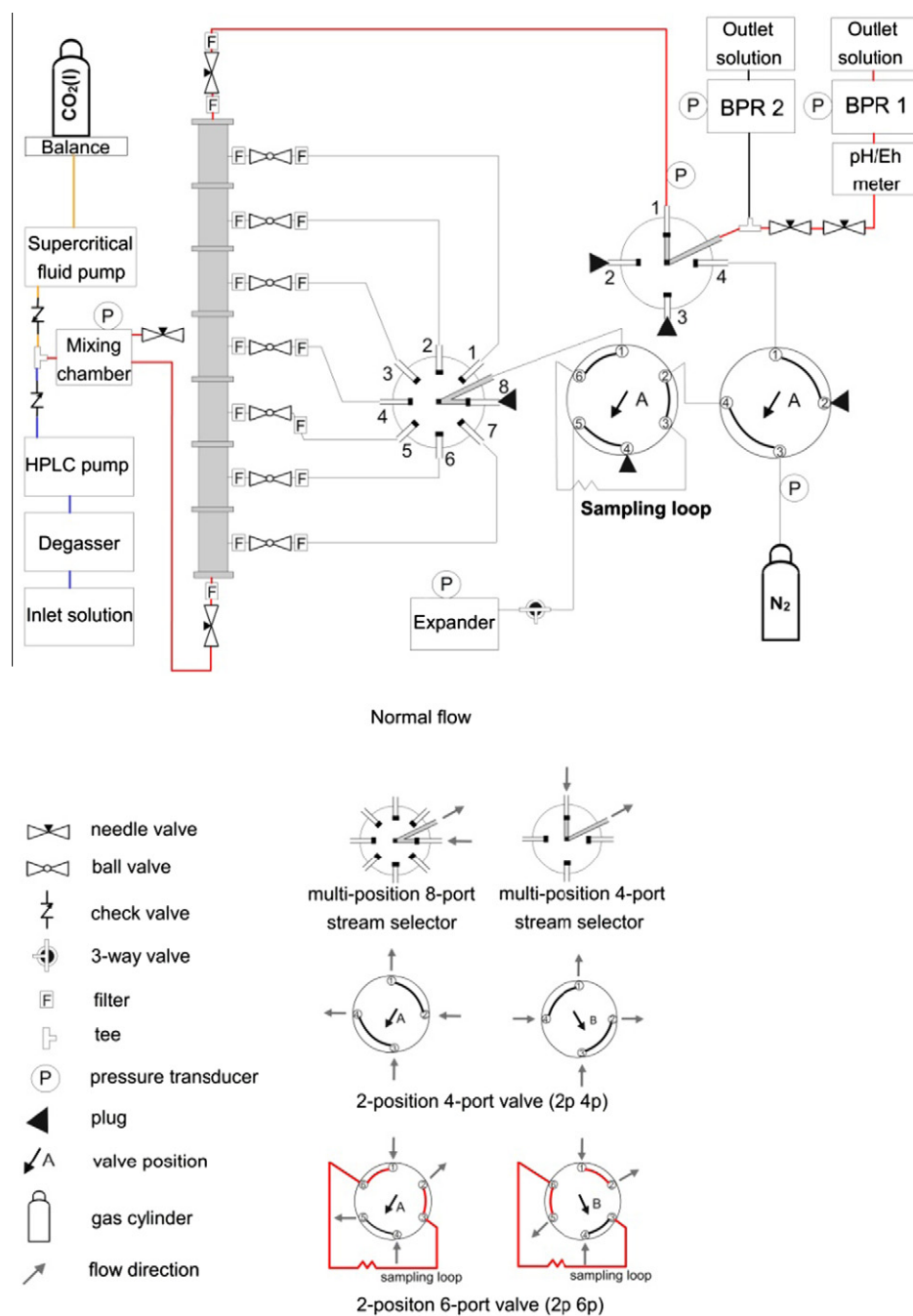

Fig. 2a. Set-up for normal flow. The CO_2 is mixed with H_2O and pumped through the column. The reacted solution passes the multi-position 4-port stream selector through port 1, which is connected to the outlet port and flows through high temperature/high pressure electrodes followed by a back pressure regulator (BPR 1). The multi-position 8-port stream selector is aligned with port 8. Both, the 2-position 6-port and 2-position 4-port valves are set on position A. All the compartment outlet ball valves are closed.

into a brine. The advantage of a reactor versus mixing loop is the option of measuring initial DIC *in situ* before the fluid comes into contact with the solid.

Depending on the desired overall flow rate of the experiment, which in the case of a large, meter-long plug may amount to several mL/min, a minimum mixing volume is needed to provide an adequate residence time for full dissolution of $CO_{2(l)}$ in water. At a flow rate of 5 mL/min and vigorous stirring (300 rpm) at 22 °C, the residence time of 20 min in the 100 mL Ti reactor was observed to be sufficient. Mixing efficiency was tested at different pump flow rates of H_2O and CO_2, i.e., different flow rate ratios yielding different initial DIC concentrations. A minimum of ten consecutive stable DIC determinations close to the expected, theoretical DIC concentrations indicated full dissolution of $CO_{2(l)}$ When the $CO_{2(l)}$ was not fully dissolved, large variations in the DIC measurements and deviations from the theoretical concentrations were noticed. A reactor volume of 100 mL as required in this study is a large mixing volume which puts some constraint on the option of alternatively using a mixing coil as it would, under the experimental conditions, correspond to ⩾55 m of inert tubing (regular 1/8″ tubing with an ID of 0.06″ yields a volume of 1 mL for every 55 cm length) that would have to be cooled/heated evenly.

When mixing $CO_{2(l)}$ and water in the mixing chamber, it is vital to avoid backflow of the H_2O–CO_2 mixture into the CO_2 pump. This corrosive liquid may destroy the upper pump head check valves which are made of SS. Potential backflow into the CO_2 pump head can also cause freezing of the solution and thus create ice particles and scratch the glass pistons. In preliminary tests a regular Tee (a unit connecting two flow paths into one) was used to combine the $CO_{2(l)}$ and the DI water lines (Fig. 2a). From there, the H_2O–CO_2 mixture flowed to the mixing reactor. However, it is recommended to keep CO_2 and DI water lines separated because the water pump runs at larger flow rates that could potentially push water into the CO_2 line. Furthermore, check valves (Swagelok®) have to be inserted before the CO_2 and DI water reactor inlets (Fig. 2). Commonly used SS check valves have a disadvantage of rubber O-rings which are not fully resistant to CO_2 attack. Stainless

steel ball check valves without O-ring or Teflon soft seated check valves (Maximator®, HiPressure Equipment Company) are better to provide longer lifetime.

Another critical issue is the flow rate ratio between the supercritical fluid (SCF) pump and water pump (high pressure liquid chromatography pump, HPLC). This ratio depends on the solubility of $CO_{2(l)}$ in water which decreases with increasing temperature and ionic strength of the solvent and increases with CO_2 partial pressure (pCO_2). Based on the literature, the mole fraction solubility of $CO_{2(l)}$ in DI water under close-to operating conditions (25 °C and 7.5 MPa total pressure) equals 0.0244 (Teng and Yamasaki, 2002) and 0.0245 (Duan et al., 2006), respectively. This value cannot be surpassed to ensure saturation and a one-phase flow of water and $CO_{2(aq)}$ into the plug. In order to calculate the appropriate pump rate ratios the following three equations are introduced: The mole fraction X_{CO_2}:

$$X_{CO_2} = \frac{nCO_{2(aq)}}{nCO_{2(aq)} + nH_2O} \tag{1}$$

where nCO_2 and nH_2O are the moles of $CO_{2(aq)}$ and H_2O, respectively. This ratio is necessary to calculate the mole ratio between H_2O and $CO_{2(aq)}$, $X_{\frac{H_2O}{CO_{2(aq)}}}$ (40.15). The molar volume (V_m) ratio between H_2O and CO_2 is calculated based on the density (δ) of H_2O and CO_2 at 25 °C and the molecular weight of both:

$$V_{m\frac{H_2O}{CO_2}} = \frac{\frac{m_{weight\ H_2O}}{\delta H_2O}}{\frac{m_{weight\ CO_2}}{\delta CO_2}} = \frac{\frac{18}{0.997}}{\frac{44}{0.77}} = 0.32 \tag{2}$$

Combining Eqs. (1) and (2), the ratio between HPLC and SCF pump flow rates to reach maximum dissolved carbon concentration is:

$$\text{Pump flow rate ratio}_{\frac{HPLC}{SCF}} = X_{\frac{H_2O}{CO_{2(aq)}}} * V_{m\frac{H_2O}{CO_2}} = 40.15 * 0.32$$

$$= 12.85 \tag{3}$$

This number means that at least 13 times more H_2O versus $CO_{2(l)}$ volume has to be delivered per time unit to ensure complete dissolution of $CO_{2(l)}$ in the Ti mixing reactor. This ratio will increase
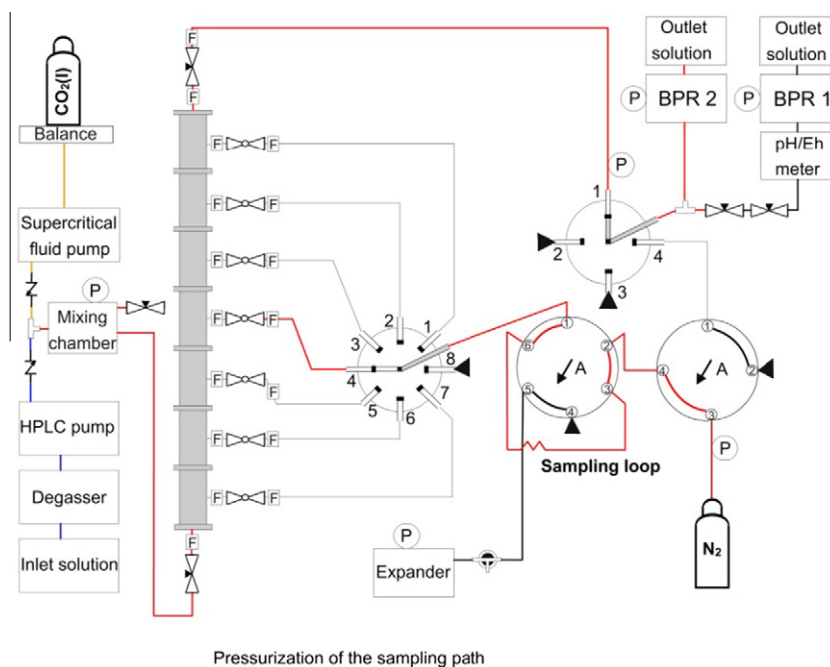

Pressurization of the sampling path

Fig. 2b. Set-up for pressurization of the sampling path with N_2. The reacted solution flows through the multi-position 4-port stream selector and the by-pass back pressure regulator (BPR 2). The multi-position 8-port stream selector is set on a chosen sampling compartment. N_2 passes the 2-position 4-port valve, the 2-position 6-port valve with the sampling loop and reaches the ball valve on the compartment sampling outlet.
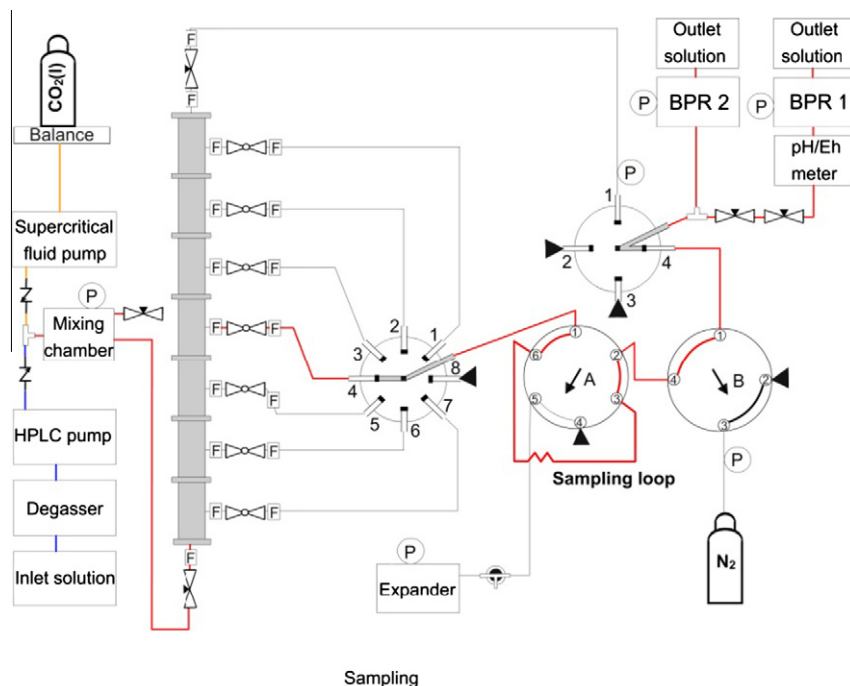
Sampling

Fig. 2c. Set-up for sampling mode, in this case from compartment #4. The multi-position 4-port stream selector is set on port 4. The solution in the column outlet line is stagnant during this stage. The ball valve of the sampled compartment is opened; solution flows through the multi-position 8-port stream selector and passes the 2-position 6-port valve in position A followed by the 2-position 4-port valve in position B. The fluid flows through the multi-position 4-port stream selector to the by-pass back pressure regulator BPR 2. After taking a sample for major ions, the fluid is diverted to the cross and BPR 1 for pH/Eh measurements.

significantly when mixing a very saline solution with $CO_{2(l)}$ and when temperature is increased. Under such circumstances, a syringe pump rather than the piston pump utilized in this study is required to deliver the very small volumes of liquid/supercritical CO_2.

3.3. Sampling the plug

Sampling of fluids is carried out by either diverting the selected stream through a stream selector to a pressurised sampling loop and expander for DIC analysis or towards the fluid sampling outlet
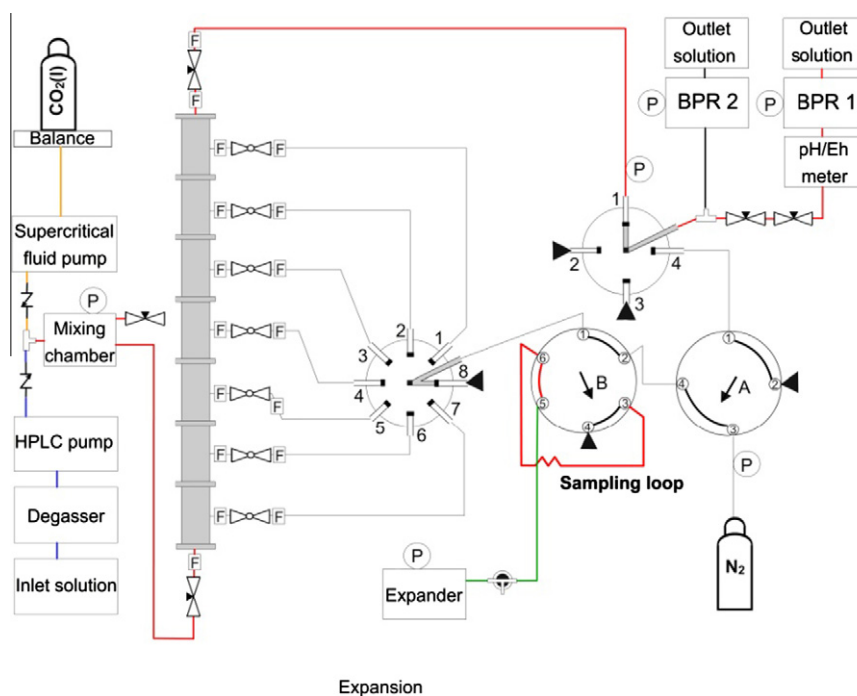

Expansion

Fig. 2d. Set-up for the expansion mode to measure the total dissolved inorganic carbon (DIC). The outlet solution is directed to pass through the multi-position 4-port stream selector set on port 1 and flows through the high temperature/high pressure electrodes followed by the back pressure regulator BPR 1. The multi-position 8-port stream selector is aligned with port 8. The 2-position 6-port valve is switched to position B which allows CO_2 expansion into the expander. The 2-position 4-port valve is switched back to position A after CO_2 expansion.

and pH and Eh electrodes (Fig. 2). The sampling unit shown in Figs. 2a–2d starts with an HC multi-position 8-port stream selector (VICI®) where individual ports are connected to corresponding column compartment outlets through 1/8″ tubing (PEEK). The selector outlet is connected to an HC 2-position 6-port valve (VICI®). In sampling mode, $CO_{2(aq)}$ is captured in a sampling loop of known volume. The DIC concentration is measured in a 26 mL custom-made plastic container, the so-called 'expander' equipped with a pressure transducer (OMEGA®) that records the pressure induced by CO_2 expansion. Following the 2-position 6-port valve, the solution flows through an HC 2-position 4-port valve (VICI®) connected to a N_2 gas cylinder. This inert gas provides pressurization of the sampling path before reactive solution is sampled to avoid degassing of CO_2 from the column. The main outlet of the column as well as the 2-position 4-port valve are connected to an HC multi-position 4-port stream selector (VICI®). From this selector outlet, the fluid passes either through a SS cross (Swagelok®) with high pressure/temperature SS pH and Eh electrodes (Corr Instruments, Texas) and finally through the main back pressure regulator (BPR 1, Swagelok®) or is by-passed to a second similar BPR 2. The addition of a second BPR and two 1/8″ inlet needle valves (one of Ti from Collins Instrument; one of SS from Swagelok®) provide the possibility for short-cutting the pH/Eh cross for calibration and/or maintenance purposes. Samples for major cations are taken from the by-pass BPR 2 to avoid long contact times of the fluid with the pH/Eh cross which is made of SS.

There are four running modes of the column. During normal flow the solution flows through the column without sampling (Fig. 2a). Preparation of the system for sampling follows by pressurizing the sampling path which, after previous sampling, remained depressurized (Fig. 2b). The third stage is the actual sampling (Fig. 2c) followed by the last stage – expansion, when the CO_2 concentration is measured in the expander (Fig. 2d).

First stage (Fig. 2a). The solution is continuously delivered to the column. In the first stage the multi-position 8-port stream selector is oriented towards the eighth port which is closed with an SS 1/8″ plug (VICI®). Subsequently, the multi-position 4-port stream selector is oriented to the first port so that, after exiting the column (ball valves on each compartment are closed), the solution flows directly via the pH and Eh cross through the BPR 1 (Fig. 2a). The pressure on the additional by-pass BPR 2 is set slightly higher than the pressure on the regular BPR 1 to divert fluid through the latter.

Second stage (Fig. 2b). Sampling preparation procedure requires orienting the multi-position 8-port stream selector to any port which is connected to a specific column compartment. Nitrogen gas fills the passage through the three lower valves in Fig. 2b, including the sampling loop, up to the compartment ball valve. Fig. 2b depicts preparation for sampling from the fourth outlet. Gas is introduced to the system until the pressure in the sampling path approaches a pressure around 2 MPa lower than the operating system pressure allowing the fluid from the column to replace the N_2 gas. During this stage the pH/Eh cross is short-cut by closing one of the two inlet cross valves and reducing the pressure on the by-pass BPR 2.

Third Stage (Fig. 2c). Sampling commences with opening the compartment ball valve. Fig. 2c represents sampling from the fourth outlet. Liquid flows through all valves from the fourth outlet and displaces the N_2 which exits the system through the by-pass BPR 2. It is important to run the initial part of the sampling phase through the by-pass BPR 2 to avoid displaced N_2 from entering and potentially persisting in the pH/Eh cross. Note that the positions of the multi-position 4-port stream selector and 2-position 4-port valve have to be changed between stage 2 and 3 (Figs. 2b and 2c) and the pressure difference between both has to be readjusted. It is during the third stage that fluid samples for subsequent

elemental and ion analysis are collected from the by-pass BPR 2 and in-line pH/Eh measurements are carried out from BPR 1.

Fourth stage (Fig. 2d). The fourth stage involves expansion of ex-solved CO_2 ($CO_{2(g)}$) from the pressurized fluid in the sampling loop into the expander (2-position 6-port valve is set on position B). The expander is maintained at atmospheric pressure prior to sampling and thus the pressure increase through expansion is recorded. At the same time the settings from the normal flow mode are restored (Fig. 2d). After measuring the CO_2 concentration the 2-position 6-port valve goes back to position A. After sampling, the tubing between the column and the 8-port multi-position stream selector is filled with solution. It is vital to prevent precipitation of secondary phases in the sampling tubing. Secondary solids cannot only clog the tubing but also change the chemistry of the sampled liquid by dissolving during the next sampling. The design of the set-up allows disconnecting the tubing after finishing the sampling procedure and flushing it with DI water and/or drying it with N_2 gas.

3.4. Analysis

To characterize the H_2O–CO_2 system chemically, two out of six parameters have to be measured: pH, pCO_2, alkalinity, DIC, HCO_3^- and CO_3^{2-}. The selection of measured parameters is related to the experimental design and conditions. High CO_2 pressure used in carbon sequestration laboratory experiments and field applications requires the *in situ* determination of the desired parameters before exposing the pressurized H_2O–CO_2 mixture to the atmosphere where CO_2 degassing can cause changes in these parameters. In this study high pressure/temperature SS pH and Eh electrodes (Corr Instruments, Texas) are used combined with an expander–transducer set-up to determine the pH and DIC, respectively. Precision of the pH/Eh measurements are ±0.1 log unit. When pH and DIC are known, alkalinity, pCO_2, HCO_3^-, and CO_3^{2-} can be recalculated using geochemical modelling software, such as PHREEQC (Parkhurst and Appelo, 1999). There are different analytical ways of DIC determination, e.g., titrimetry, ion chromatography, or standard addition technique. In this study, the $CO_{2(aq)}$ is captured in a sampling loop of know volume (1 mL) as depicted in Fig. 2d. A pressure transducer (OMEGA®) connected directly to an expander measures the pressure change induced by CO_2 expansion. Recalculations of ΔP made by CO_2 expansion yield DIC, according to:

$$\text{Volume of } CO_2 \ (mL) = [(P_{\exp} - P_{atm}) * \text{volume of expander}]/P_{atm} \tag{4}$$

$$\text{DIC}\left[\frac{\text{mol}}{\text{L}}\right] = \frac{\frac{\text{volume of } CO_2 \ (mL)}{\text{molar volume of } CO_2 \ \left[\frac{L}{\text{mol}}\right]}}{\text{volume of the sample (mL)}} \tag{5}$$

where P_{atm} is the atmospheric pressure in the expander prior to CO_2 expansion and P_{exp} is the final pressure after expansion. Both values are relayed through the transducer to an appropriate analog signal reader (DP41-B, OMEGA®). This technique is very fast, simple and gives comparable results with other analytical methods. In this study, results from the expander–transducer method were compared with the standard addition technique (SAT, Table 1). The set-up for the SAT method is shown in Fig. 3. This method was successfully employed in a related study dealing with fluid carbonation (Alfredsson et al., 2011). The SAT method determines the DIC concentration by repeated pH measurements of a concentrated base (0.5 M KOH) into which CO_2 from a sampled solution has been repeatedly degassed. The pH electrode records the pH change as a function of the sampled volume. With each sample being captured into the base the pH is lowered. Delta pH is recalculated to the amount of consumed moles of OH by the dissociation of H_2CO_3, thus yielding the molar carbonate concentration. This technique works only in a pH range where CO_3^{2-} is the predominant aqueous carbon

Table 1
Comparison between calculated theoretical concentrations of DIC and concentrations determined by the standard addition technique (SAT) and the expander–transducer method (see text). The reproducibility test was performed at a H_2O/CO_2 pump ratio of 16. The percentage recovery for the two methods has also been added.

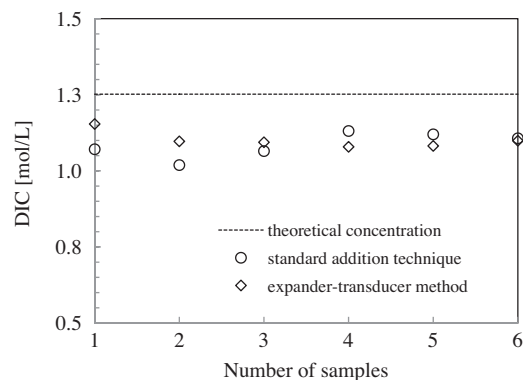| DIC concentration (mol/L)			Percent recovery (%)	
Theoretical	SAT	Expander	SAT	Expander
1.25	1.07	1.15	86	92
1.25	1.02	1.10	81	88
1.25	1.06	1.09	85	87
1.25	1.13	1.08	90	86
1.25	1.12	1.08	89	86
1.25	1.11	1.10	88	88

Fig. 4. Comparison between theoretical and measured DIC at the H_2O/CO_2 flow rate ratio of 16. Measured concentrations were obtained with the standard addition technique and the expander–transducer method, respectively.

species ($\geqslant 12.5$) and only if gas is sampled. For the expander–transducer method to work, the pH of the fluid which is sampled has to be relatively low (<5.5) such that all inorganic carbon species are mainly present as $CO_{2(aq)}$. If the pH increases due to fast mineral or glass dissolution in the plug, the contribution from HCO_3^- to the overall inorganic carbon species may become important and other methods, e.g. titration, will be more suitable for the DIC determination. Alternatively, acid could be injected into the loop after degassing to convert any HCO_3^- into $CO_{2(g)}$ and drive it out of the loop and into the expander.

Further laboratory tests confirming the accuracy of the expander–transducer method were carried out at 22 °C and 8 MPa total pressure (Fig. 3). The tests (and subsequent column experiment) were performed under known H_2O/CO_2 pump ratios at 8 MPa to provide ~1 MPa pressure buffer with respect to potential CO_2 boiling of $CO_{2(l)}$ prior to mixing which is a reasonable safety margin

in complicated pressure systems where small pressure fluctuations always occur. According to CO_2 solubility in water (Teng et al., 1997), theoretical DIC concentrations were calculated for selected H_2O/CO_2 pump flow rate ratios. The theoretical concentration at a H_2O/CO_2 pump flow rate ratio of 16 was compared with measured values obtained with the expander–transducer method as well as with SAT (Table 1 and Fig. 4). Additionally, the DIC was measured with the expander method at varying initial inlet CO_2 concentrations where the H_2O pump flow rate remained constant and only the CO_2 pump flow rate was changed. Results of these tests indicate that the obtained average recovery at different H_2O/CO_2 pump flow rate ratios equals 95%. At higher H_2O/CO_2 flow
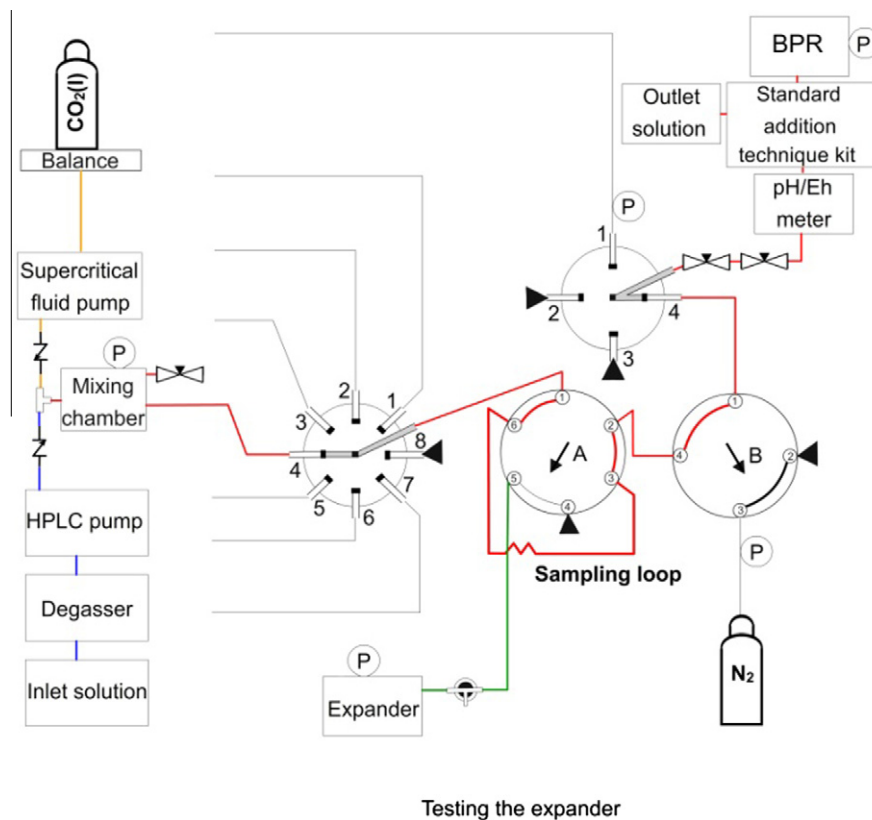

Fig. 3. Set-up for DIC measurement via standard addition technique (SAT). The CO_2 is mixed with H_2O and flows in chronological order through the following key components: the multi-position 8-port stream selector, the 2-position 6-port valve (position A), the 2-position 4-port valve (position B), the multi-position 4-port stream selector, the pH/Eh cross, the standard addition technique kit (where the DIC measurement is performed), and the back pressure regulator (BPR 1). An alternative DIC analysis is carried out in the expander as shown in Fig. 2d.

Table 2
The DIC concentrations obtained with the expander–transducer method. Comparison between measured DIC (DIC_m) at different pre-set H_2O/CO_2 flow rate ratios with the theoretical DIC concentrations (DIC_{th}) calculated for the tested flow rate ratios.

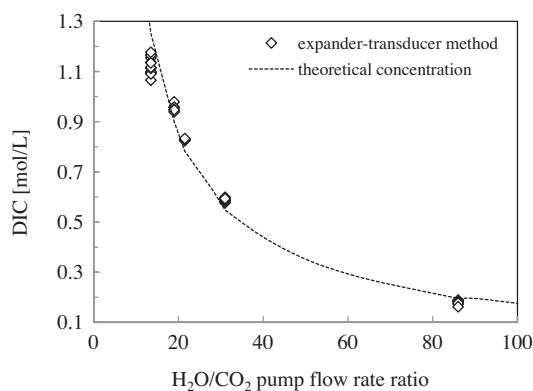| H_2O pump flow rate (mL/min)	CO_2 pump flow rate (mL/min)	Pump ratio H_2O/CO_2	DIC_m (mol/L)	Number of measurements	Standard deviation	Relative st. dev. (%)	DIC_{th} (mol/L)	Percent recovery (%)
5.00	0.32	16	1.10	16	0.04	3.81	1.25	87
5.00	0.23	22	0.95	6	0.01	1.44	0.90	101
5.00	0.20	25	0.83	6	0.04	0.34	0.78	101
5.00	0.14	36	0.59	10	0.01	1.42	0.55	103

Fig. 5. Relationship between H_2O/CO_2 pump flow rate ratios and the DIC obtained with the expander–transducer method. At higher flow rate ratios ($\geqslant 22$), measured concentrations closely match the theoretical DIC. The theoretical curve was calculated based on the solubility mole fraction of CO_2, molar volume ratios of H_2O and CO_2, and theoretical pump flow ratios (cf. Eqs. (1)–(3)).
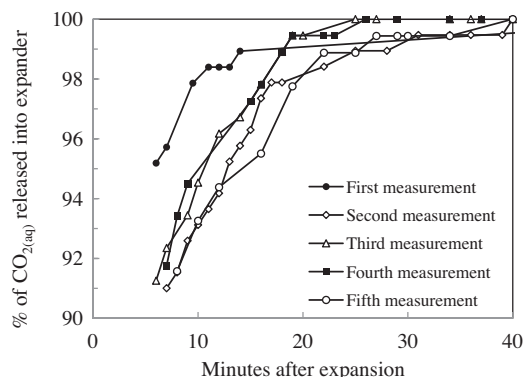

Fig. 6. Efficiency of CO_2 expansion. After 20 min, 98% of $CO_{2(aq)}$ captured from the sampled solution degassed into the expander, indicating the critical minimum response time for pressure reading from the transducer which yields the DIC concentration according to Eqs. (4) and (5).

4. Results

The system was tested at 22 °C and 8 MPa total pressure. The column was filled with basaltic glass grains 40–100 μm in diameter. The DI water at a flow rate of 3.5 mL/min and $CO_{2(l)}$ at a flow rate of 0.22 mL/min were mixed and pumped through the column
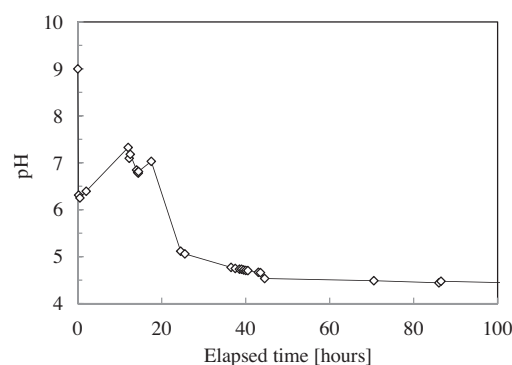

Fig. 7. Evolution of the pH in the column during the replacement of the initial DI solution with the 1.2 M $CO_{2(aq)}$ solution. Values were measured in the outlet of the column. First point on the plot (pH 9) represents the column outlet pH during DI water conditioning of the basalt slurry.

for 91 h. Initial DIC concentration was ~1.2 mol/L and initial, measured pH 3.2 at 22 °C.

The experiment started with DI water being pumped through the HPCFR at 22 °C and 0.1 MPa to condition the system. Then, the total/hydraulic pressure was increased to 8 MPa by adjusting the BPR 1 and BPR 2 accordingly, followed by turning on the $CO_{2(l)}$ pump. It took approximately 44 h (5 pore volumes) to replace the initial reacted solution of pH ~ 9, which is the result of DI water–basaltic glass interaction in the column, with the H_2O–CO_2 mixture and decrease the pH to ~4.5 (Fig. 7). First samples of the solute from all the outlets were taken after 44 h followed by a second set after 90 h. During the sampling the pH, Eh and DIC were determined in-line which correspond to *in situ* values. The outlet solution was sampled, filtered using a 0.2 μm cellulose acetate filter, and then acidified with concentrated supra-pure HNO_3 prior to analysis for major elements with ICP-OES (Inductively Coupled Plasma Optical Emission Spectrometry). Analytical uncertainties of ICP-OES analyses are in the order of $\leqslant 5\%$. Results of the chemical analyses are reported in Table 3. A comparison of major cation concentrations between individual compartments is depicted in Fig. 8. Elemental concentrations for Si, Ca, Mg, Al, and Fe increased by factors of 11, 35, 20, 9 and 2500 after 48 h and by factors of 8, 12, 12, 22 and 1800 after 90 h of experiment duration compared to elemental concentrations during conditioning of the basaltic glass slurry with DI water. The DIC concentration and pH remained constant along the flow path.

5. Discussion

The HPCFR was designed to monitor the evolution of the solute chemistry over different time stages along the flow path under high total/pCO_2 pressure. There are many challenges related to the experimental set-up which have to be overcome. A major problem in liquid or supercritical CO_2 experiments is the corrosive properties of the CO_2 charged water. Various kinds of less corrosion

rate ratios ($\geqslant 22$), recovery reached 100%, assuming that the H_2O pump and the CO_2 pump are delivering solutions with the same precision at different flow rate ratios (Table 2 and Fig. 5). Average recovery at the flow rate ratio of 16 reaches only 87%. The time required to yield $\geqslant 98\%$ recovery of the CO_2 degassing from the sampling loop into the expander is at least 20 min (Fig. 6).

Table 3
Results of H_2O–CO_2–basaltic glass interaction in different compartments within the column. The pH and Eh were measured in-line and major cations with ICP-OES. The DIC concentration was obtained with the expander–transducer technique. Initial cation concentrations correspond to the conditioning phase of the column, when only DI water was pumped through.

Sample	Compartment	Elapsed time (h)	pH		Eh (mV)	DIC (mol/L)	Si		Ca		Mg		Al		K		Na		Fe	
			Initial	CO$_{2exp}$			Initial	CO$_{2exp}$	Initial	CO$_{2exp}$	Initial	CO$_{2exp}$	Initial	CO$_{2exp}$	Initial	CO$_{2exp}$	Initial	CO$_{2exp}$	Initial	CO$_{2exp}$
							(mmol/kg)													
P 7 1	7	44.5	9.27	4.53	164	1.24	0.17	1.83	0.04	1.39	0.04	0.81	0.05	0.45	0.00	0.19	0.00	0.16	0.00	0.25
P 6 1	6	45.5	9.32	4.48	175	1.20	0.17	1.63	0.04	0.90	0.04	0.66	0.05	1.00	0.00	0.12	0.00	0.12	0.00	0.21
P 5 1	5	46.5	9.31	4.48	169	1.20	0.16	1.45	0.04	0.66	0.04	0.55	0.05	1.13	0.00	0.07	0.00	0.11	0.00	0.19
P 4 1	4	47.5	9.37	4.47	179	1.20	0.16	1.26	0.04	0.55	0.04	0.50	0.05	1.06	0.00	0.04	0.01	0.09	0.00	0.17
P 3 1	3	48.5	9.39	4.52	177	1.20	0.15	1.07	0.04	0.45	0.04	0.42	0.05	0.95	0.00	0.02	0.00	0.09	0.00	0.16
P 2 1	2	49.5	9.34	4.55	196	1.21	0.14	0.78	0.03	0.37	0.03	0.34	0.04	0.76	0.00	0.01	0.00	0.07	0.00	0.14
P 1 1	1	50	9.12	4.55	189	1.19	0.07	0.43	0.02	0.31	0.02	0.25	0.02	0.44	0.00	0.01	0.00	0.06	0.00	0.11
P 7 2	7	86.5	9.27	4.48	186	1.16	0.17	1.40	0.04	0.48	0.04	0.47	0.05	1.12	0.00	0.04	0.00	0.10	0.00	0.18
P 6 2	6	87.5	9.32	4.47	187	1.16	0.17	1.28	0.04	0.43	0.04	0.42	0.05	1.07	0.00	0.03	0.00	0.09	0.00	0.17
P 5 2	5	88	9.31	4.46	184	1.16	0.16	1.17	0.04	0.39	0.04	0.40	0.05	0.99	0.00	0.02	0.00	0.08	0.00	0.16
P 4 2	4	88.5	9.37	4.46	184	1.17	0.16	1.04	0.04	0.33	0.04	0.36	0.05	0.90	0.00	0.02	0.01	0.07	0.00	0.14
P 3 2	3	89	9.39	4.45	191	1.17	0.15	0.87	0.04	0.29	0.04	0.31	0.05	0.77	0.00	0.01	0.00	0.07	0.00	0.14
P 2 2	2	90	9.34	4.44	179	1.15	0.14	0.63	0.03	0.23	0.03	0.26	0.04	0.57	0.00	0.01	0.00	0.06	0.00	0.12
P 1 2	1	91.5	9.12	4.44	192	1.15	0.07	0.28	0.02	0.16	0.02	0.17	0.02	0.28	0.00	0.00	0.00	0.04	0.00	0.09

resistant materials such as O-rings and plastic seals in BPR and check valves can be irreversibly damaged when continuously exposed to $CO_{2(aq)}$ for a long time. Worse, there is no possibility for replacement if needed because of the required pressure relief. Degassing of the system takes a long time and during degassing and re-launching of the experiment the chemistry of the system may change and influence secondary phase precipitation. The CO_2 charged water not only reduces the lifetime of vital parts in the experimental set-up but may also lead to damage of the pH electrodes. The CO_2 can diffuse into the inner compartment of the reference probe. Even though this does not change the probe potential, it may cause mechanical damage to the inner probe compartment during sudden pressure drops. Small pressure drops are unavoidable during the sampling procedure when the stream selectors are switched from one position to the other and, therefore, there is always a risk of inaccurate pH measurement. The manufacturer's recommended lifetime of the pH/Eh electrodes is about 6 months but heavily dependent on the system temperature. Another issue is clogging of the compartments' outlet filters with fine material from the column (Fig. 1, Box 6). Clogged filters can result in a 1–1.5 MPa pressure surge immediately after insertion, and if clogging persists during the whole experimental duration, it may not be possible to sample the compartment outlet and information from that particular compartment will be lost. Pumps delivering CO_2 and H_2O can also pose a problem. In particular, the supercritical CO_2 pump is susceptible to damage when in-line check valves start to leak, consequently allowing backflow of the aqueous solution into the CO_2 pump. Such backflow inevitably causes deterioration of the pump leading to fluctuating flow rates, incontrollable inlet conditions, and ultimately costly downtime and repair. A syringe pump may thus be a more suitable solution for $CO_{2(l)}$–$CO_{2(aq)}$–rock experiments, especially when dealing with low flow rates.

Other, non-technical issues involve sampling effects on the system flow. Taking a sample perturbs the overall vertical flow in the system. Therefore, sampling of the individual compartments is kept as short as possible to keep the disturbance of the flow dynamics and solute chemistry small. During sampling, fluid, which is above the sampled compartment, does not move. In order to avoid sampling a stagnant fluid the sampling protocol commences with the uppermost compartment and moves downwards.

Despite these technical and hydrological drawbacks, during this first phase of CO_2 pulse in the column, which mimics the onset of CO_2 injection in the field, a clear consistent elemental behavior is observable.

After 90 h (12 pore volumes), concentration curves start to overlap which is interpreted as the approach of steady-state dissolution of the basaltic glass. Steady-state dissolution in flow through reactors is commonly defined as a constant outlet concentration of a conservative element (e.g. Si) from the solid at constant flow rate. Apparently, steady-state was not attained in the HPCFR but nonetheless the silica concentration at the second point was taken as a point of reference to determine a preliminary, close-to steady-state dissolution rate of the basaltic glass in the column and compare that value with literature rates. The experimentally determined dissolution rate normalized to geometric surface area (290 cm^2/g) yielded $10^{-13.4}$ mol$_{Si}$/cm^2/s^{-1} and compares quite favorably with a calculated dissolution rate of $10^{-13.3}$ mol$_{Si}$/cm^2/s^{-1} based on a rate expression given by Gislason and Oelkers (2003). So while the system may not have reached steady-state, its preliminary dissolution rate determined from the silica outlet concentration is very consistent with the far-from-equilibrium dissolution of basaltic glass of similar composition under acidic conditions of pH 4.5 and ambient temperature.

Further, one dimensional reactive transport modelling was carried out using PHREEQC (Parkhurst and Appelo, 1999) and the llnl.dat database. Results of the calculations were again compared with the experimental solute data. In the simulation, the column was divided into seven cells (dimensions of the cells represented the real scale of the compartments) and the flow of the fluid was directed from the first to the seventh cell. DI water saturated with 1.2 M $CO_{2(aq)}$ was used as the initial solution and allowed to react with basaltic glass in accordance with the dissolution rate expression reported by Gislason and Oelkers (2003) and previously implemented to compare dissolution rates. The total surface area of the basaltic glass used in the simulation was set as one tenth of the geometric surface area (29 cm^2/g) and the time step corresponded to one residence time in the compartment.

Results of the geochemical modelling are summarized in Fig. 9 and reveal an increase of the individual elemental concentrations along the flow path from the first to the seventh compartment which agrees well in magnitude with the experimental results. The major increase in solute concentrations is from the reactor inlet to the first cell/compartment outlet and decreases further along the flow path which is also reflected in the experimental data. The only discrepancy appears in the pH which is between 0.6 (in the seventh compartment) and 1.0 (in the first compartment) log units lower than experimental values. In addition, in the geochemical simulation steady-state is attained after only 10 h of experiment
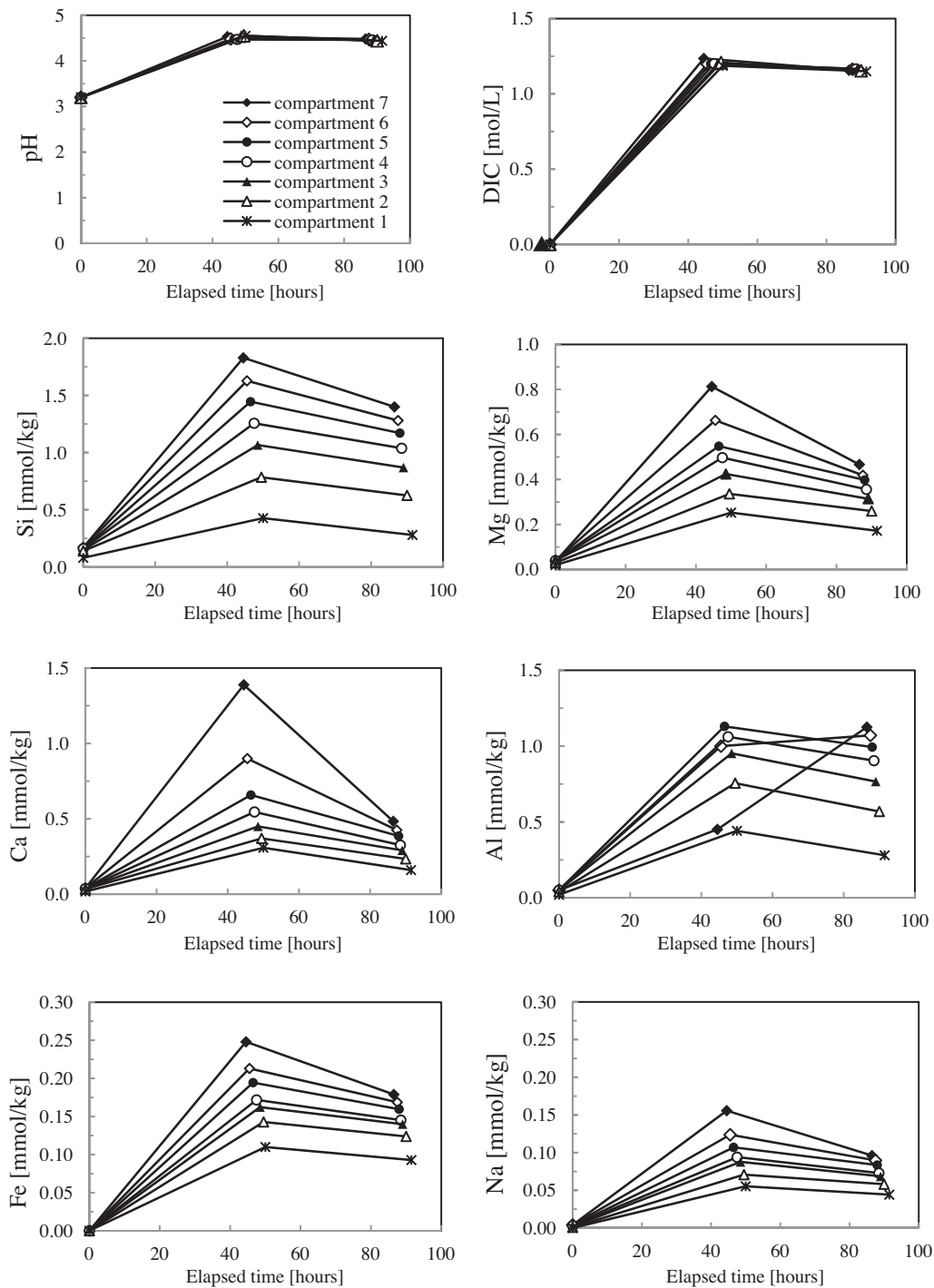
Fig. 8. Results from the chemical analyses of the individual compartments during CO$_2$ injection. The compartment number reflects the sampling distance along the flow path inside the column, starting with compartment 1 which is the closest to the inlet of the column. The first set of points in the pH plot represents the initial pH of the H$_2$O–CO$_2$ solution in the mixing reactor before entering the column. The first set of points on the other plots represents the elemental concentrations during the conditioning of the column, when only DI water was pumped through.

duration, in stark contrast to the +90 h in the experiment. Reducing the geometric surface area from 290 to 29 cm^2/g resulted in exceptional agreement between major elemental concentrations along the flow path in the model calculations versus the experimental data. The real reactive surface area of basaltic glass inside the column is unknown due to possible preferential flow, changes in the grain morphology and size during experiment duration, secondary phase precipitation and hydraulic pressure exerted on the solid. Gysi and Stefánsson, 2012b found that a 10-fold decrease in geo-

metric surface area of their basaltic glass used in the simulation resulted in shifting the overall reaction path to over 100 days indicating that the reactive surface area plays a pivotal role in controlling basaltic glass dissolution kinetics. In the reactive transport modelling simulation of a field CO$_2$ injection into basaltic basement, Aradóttir et al. (2012) assumed the reactive surface area of minerals and glasses to be 20 cm^2/g alike, which is close to the surface area applied in this study. Occurrence of preferential flow in the column is a major unknown and cannot be ruled out unambig-
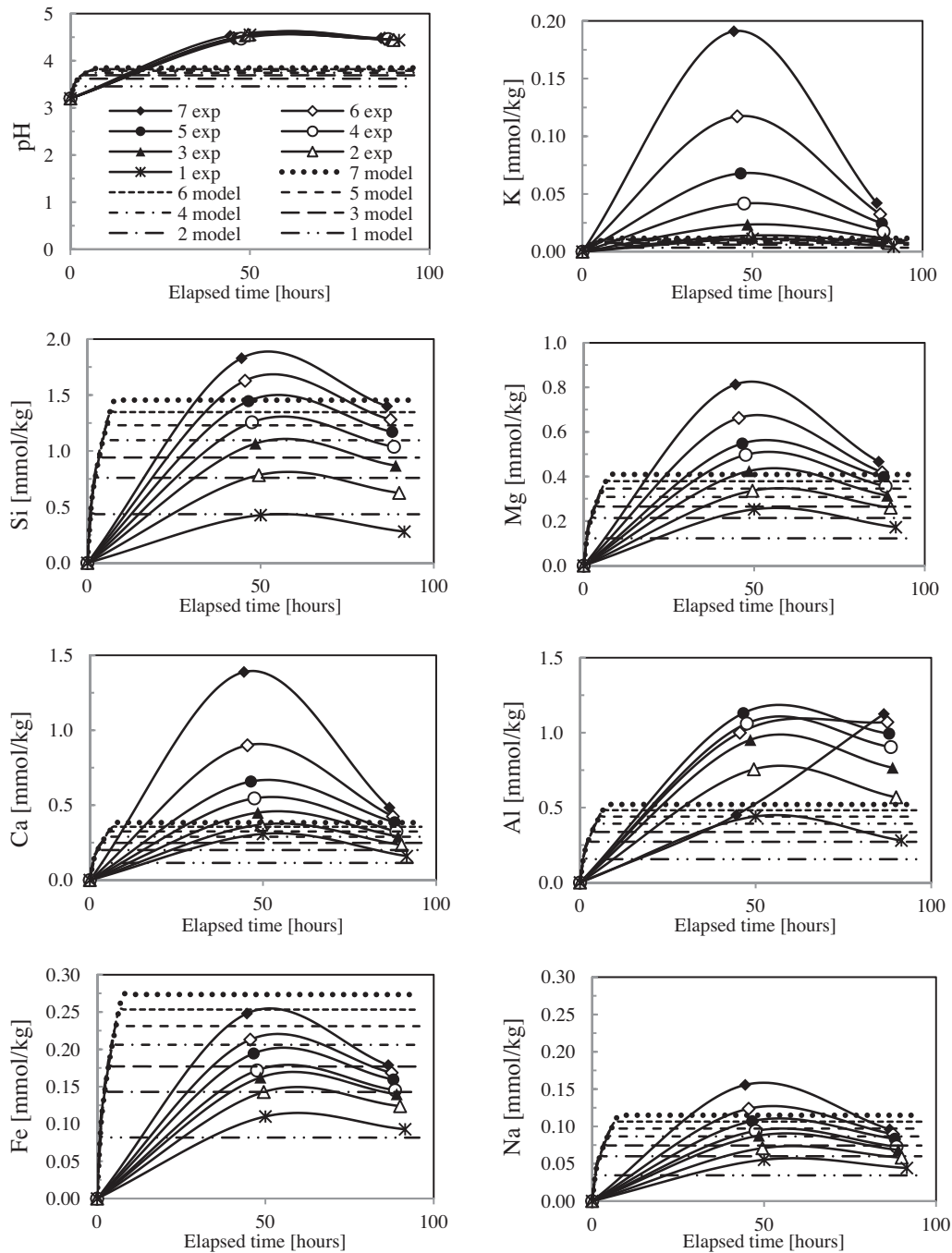
Fig. 9. Comparison between results of geochemical modelling and experiments showing the concentration of major cations and pH. The symbols represent the experimental results ('exp' in the legend) and the dashed lines represents outcome of reactive transport modelling ('model' in the legend) for each compartment. The initial DIC concentration used in the simulation was 1.2 M and the total surface area of the basaltic glass implemented in the simulation was one tenth of the geometric surface area (29 cm^2/g). The dissolution rate expression for basaltic glass was taken from Gislason and Oelkers (2003). The first set of points represents the initial concentration of the H$_2$O–CO$_2$ solution in the mixing reactor before entering the column.

uously. However, if preferential flow indeed occurred, only a fraction of the total basaltic glass surface area would be in contact with the carbonated water. It can be expected that under such conditions, the scale of dissolution and reaction kinetics would be reduced proportionately to the available reduced reactive surface area and, therefore, steady-state could be approached much earlier than +90 h. Likewise, the consistent solute chemistry evolution in Fig. 8 undermines partial preferential flow inside the column unless it affected the entire reactor uniformly, compartment by compartment, which seems unlikely.

Interestingly, the main change in the measured pH occurs in the first compartment where the initial pH of 3.2 increases to 4.5 and remains constant thereafter. This observation is all the more intriguing because the surface area of the basaltic glass up to the first compartment outlet is only 8% of the remainder of the column. Constant pH along the flow path is not surprising when taking the buffer capacity of the solution into account. The buffer capacity β is mathematically defined as ΔA or ΔB divided by ΔpH and describes the resistance of a solution to a pH change when acid (A) or base (B) are added incrementally (Urbanski and Schock, 2000). In the

case of the HPCFR, basaltic glass is the base used to titrate the carbonic acid created by $CO_{2(aq)}$ to a pH range amenable to carbonate precipitation. At an initial inlet pH around 3, the buffer capacity of the CO_2 charged solution is very low ($\sim 10^{-3}$ eq/kg) because DI water has no alkalinity and the dissolution of CO_2 does not add any alkalinity. Thus, proton consumption of this unbuffered inlet solution through dissolution reactions with the basaltic glass leads to a noticeable pH rise in the lowest part of the column. However, the buffer capacity of the solution rises exponentially with increasing pH such that over time, a constant pH evolves when the proton production by H_2CO_3 dissociation equals that of proton consumption by basaltic glass dissolution (Gislason and Eugster, 1987; Wolff-Boenisch, 2011).

Based on acidity titrations performed with PHREEQC, raising the pH from 3.2 to 4.5 through dissolution reactions with the basaltic glass increases the buffer capacity β from $10^{-2.9}$ to $10^{-2.1}$ eq/kg. A further, apparently small rise in pH from 4.5 to only 4.7 causes, however, a similar increase in β to $10^{-1.4}$ eq/kg. To enable a further increase in pH, vital for carbonate precipitation, dissolution rates of basalt and thus proton consumption have to be increased significantly. An increase in temperature from 25 to 50 °C at pH 3.5 enhances basaltic glass dissolution twofold (Gislason and Oelkers, 2003). Another way to promote basaltic dissolution kinetics is the addition of F^- to the inlet solution. Fluoride has the capability of forming aqueous complexes with Al, diminishing the dissolution rate inhibitory effect of aqueous Al^{3+}. Addition of 90 μmol of F^- to a pH 4 solution increases the dissolution rate of basaltic glass by nearly an order of magnitude (Wolff-Boenisch et al., 2004). Wolff-Boenisch (2011) discussed different scenarios on how to overcome the pH buffer hurdle, including dilution of the $CO_{2(aq)}$ solution. The constant pH observed during the experiment indicates the need for chemical and/or temperature changes to the column experiment to overcome this stalemate and induce precipitation reactions at higher pH.

6. Conclusions

The HPCFR is designed to sample pressurized gas loaded solution along the flow path within a column filled with mineral or glass particles. While its application is exemplified in this study using a carbonated solution and basaltic glass, it should also work for supercritical CO_2 applications because the system pressure is higher than the supercritical pressure of CO_2 and the experimental temperature can be regulated up to 90 °C. Furthermore the inlet part of the plug can be adjusted to accommodate gas mixtures such as CO_2–H_2S and/or CO_2–SO_2.

Sampling reactive liquid at spatial intervals and under pressure makes the HPCFR unique in comparison with other columns constructed for studies of water–rock interaction. Measuring the evolution of the crucial parameters DIC and pH in-line which correspond to in situ values in H_2O–pCO_2 or H_2O–$scCO_2$ (sc = supercritical) systems gives the set-up an additional and crucial advantage over other experimental reactor systems. Due to its complexity and size, technical challenges of the HPCFR remain and it requires daily attention and dedication during the entire experiment duration.

The solute chemistry resulting from H_2O–CO_2–basaltic glass interaction inside the column was successfully modelled by 1D reactive transport modelling indicating that the reactor is a reliable tool to investigate the behavior of pressurized CO_2 in the subsurface. Likewise, the experimentally determined dissolution rate, based on Si and normalized to the geometric surface area corresponds well with literature rates.

A first conclusion from the preliminary run with $CO_{2(aq)}$ is that the pH of the reactive fluid inside the column remains low along the flow path such that carbonate saturation is not attained. Appropriate changes to the experimental conditions are being evaluated to enhance the dissolution kinetics of the basaltic glass and to overcome the buffer capacity which is deemed the principal cause of the stagnant pH.

References

Alfredsson, H.A., Wolff-Boenisch, D., Stefánsson, A., 2011. CO_2 sequestration in basaltic rocks in Iceland: development of a piston-type downhole sampler for CO_2 rich fluids and tracers. Energy Proc. 4, 3510–3517.

Andreani, M., Luquot, L., Gouze, P., Godard, M., Hoisé, E., Gibert, B., 2009. Experimental study of carbon sequestration reactions controlled by the percolation of CO_2-rich brine through peridotites. Environ. Sci. Technol. 43, 1226–1231.

Aradóttir, E.S.P., Sonnenthal, E.L., Björnsson, G., Jónsson, H., 2012. Multidimensional reactive transport modeling of CO_2 mineral sequestration in basalts at the Hellisheidi geothermal field, Iceland. Int. J. Greenhouse Gas Control 9, 24–40.

Bateman, K., Turner, G., Pearce, J.M., Noy, D.J., Birchall, D., Rochelle, C.A., 2005. Expérimentation de longue durée sur grandes colonnes, dans le contexte du stockage géologique de CO_2: étude des interactions eau-roche et modélisation. Oil Gas Sci. Technol. – Rev. IFP, vol. 60, pp. 161–175.

Bateman, K., Rochelle, C., Lacinska, A., Wagner, D., 2011. CO_2–porewater–rock reactions – large-scale column experiment (Big Rig II). Energy Proc. 4, 4937–4944.

Bortoluzzi, D., Cinquemani, C., Torresani, E., Spilimbergo, S., 2011. Pressure-induced pH changes in aqueous solutions – on-line measurement and semi-empirical modelling approach. J. Supercrit. Fluids 56, 6–13.

Duan, Z., Sun, R., Zhu, C., Chou, I.M., 2006. An improved model for the calculation of CO_2 solubility in aqueous solutions containing Na^+, K^+, Ca^{2+}, Mg^{2+}, Cl^-, and SO_4^{2-}. Mar. Chem. 98, 131–139.

Flaathen, T.K., Gislason, S.R., Oelkers, E.H., Sveinbjörnsdóttir, Á.E., 2009. Chemical evolution of the Mt. Hekla, Iceland, groundwaters: a natural analogue for CO_2 sequestration in basaltic rocks. Appl. Geochem. 24, 463–474.

Garg, A., Shukla, P.R., 2009. Coal and energy security for India: role of carbon dioxide (CO_2) capture and storage (CCS). Energy 34, 1032–1041.

Gislason, S.R., Eugster, H.P., 1987. Meteoric water–basalt interactions. I: A laboratory study. Geochim. Cosmochim. Acta 51, 2827–2840.

Gislason, S.R., Oelkers, E.H., 2003. Mechanism, rates, and consequences of basaltic glass dissolution: II. An experimental study of the dissolution rates of basaltic glass as a function of pH and temperature. Geochim. Cosmochim. Acta 67, 3817–3832.

Gislason, S.R., Veblen, D.R., Livi, K.J.T., 1993. Experimental meteoric water–basalt interactions: characterization and interpretation of alteration products. Geochim. Cosmochim. Acta 57, 1459–1471.

Gislason, S.R., Wolff-Boenisch, D., Stefansson, A., Oelkers, E.H., Gunnlaugsson, E., Sigurdardottir, H., Sigfusson, B., Broecker, W.S., Matter, J.M., Stute, M., Axelsson, G., Fridriksson, T., 2010. Mineral sequestration of carbon dioxide in basalt: a pre-injection overview of the CarbFix project. Int. J. Greenhouse Gas Control 4, 537–545.

Gudbrandsson, S., Wolff-Boenisch, D., Gislason, S.R., Oelkers, E.H., 2011. An experimental study of crystalline basalt dissolution from $2 \leqslant pH \leqslant 11$ and temperatures from 5 to 75 °C. Geochim. Cosmochim. Acta 75, 5496–5509.

Gysi, A.P., Stefánsson, A., 2012a. CO_2–water–basalt interaction. Low temperature experiments and implications for CO_2 sequestration into basalts. Geochim. Cosmochim. Acta 81, 129–152.

Gysi, A.P., Stefánsson, A., 2012b. Experiments and geochemical modeling of CO_2 sequestration during hydrothermal basalt alteration. Chem. Geol. 306–307, 10–28.

Gysi, A.P., Stefánsson, A., 2012c. Mineralogical aspects of CO_2 sequestration during hydrothermal basalt alteration—an experimental study at 75 to 250 °C and elevated pCO_2. Chem. Geol. 306–307, 146–159.

Kelemen, P.B., Matter, J., 2008. In situ carbonation of peridotite for CO_2 storage. Proc. Natl. Acad. Sci. USA 105, 17295–17300.

Luquot, L., Gouze, P., 2009. Experimental determination of porosity and permeability changes induced by injection of CO_2 into carbonate rocks. Chem. Geol. 265, 148–159.

Matter, J.M., Takahashi, T., Goldberg, D., 2007. Experimental evaluation of in situ CO_2–water–rock reactions during CO_2 injection in basaltic rocks: Implications for geological CO_2 sequestration. Geochem. Geophys. Geosyst. 8, Q02001.

McGrail, B.P., Schaef, H.T., Ho, A.M., Chien, Y.-J., Dooley, J.J., Davidson, C.L., 2006. Potential for carbon dioxide sequestration in flood basalts. J. Geophys. Res. 111, B12201.

Munz, I.A., Brandvoll, O., Haug, T.A., Iden, K., Smeets, R., Kihle, J., Johansen, H., 2012. Mechanisms and rates of plagioclase carbonation reactions. Geochim. Cosmochim. Acta 77, 27–51.

Oelkers, E.H., Gislason, S.R., 2001. The mechanism, rates and consequences of basaltic glass dissolution: I. An experimental study of the dissolution rates of basaltic glass as a function of aqueous Al, Si and oxalic acid concentration at 25 °C and pH = 3 and 11. Geochim. Cosmochim. Acta 65, 3671–3681.

Oelkers, E.H., Gislason, S.R., Matter, J., 2008. Mineral carbonation of CO_2. Elements 4, 333–337.

Parkhurst, D.L., Appelo, C.A.J., 1999. User's Guide to PHREEQC (Version 2) – A Computer Program for Speciation, Batch-reaction, One-dimensional Transport, and Inverse Geochemical Calculations. U.S. Geol. Surv. Water-Resour. Invest. Rep. 99-4259.

Prigiobbe, V., Hänchen, M., Costa, G., Baciocchi, R., Mazzotti, M., 2009. Analysis of the effect of temperature, pH, CO_2 pressure and salinity on the olivine dissolution kinetics. Energy Proc. 1, 4881–4884.

Schaef, H.T., McGrail, B.P., 2009. Dissolution of Columbia River Basalt under mildly acidic conditions as a function of temperature: experimental results relevant to the geological sequestration of carbon dioxide. Appl. Geochem. 24, 980–987.

Stockmann, G.J., Wolff-Boenisch, D., Gislason, S.R., Oelkers, E.H., 2011. Do carbonate precipitates affect dissolution kinetics? 1: Basaltic glass. Chem. Geol. 284, 306–316.

Teng, H., Yamasaki, A., 2002. Pressure-mole fraction phase diagrams for CO_2–pure water system under temperatures and pressures corresponding to ocean waters at depth to 3000 m. Chem. Eng. Commun. 189, 1485–1497.

Teng, H., Yamasaki, A., Chun, M.K., Lee, H., 1997. Solubility of liquid CO_2 in water at temperatures from 278 K to 293 K and pressures from 6.44 MPa to 29.49 MPa and densities of the corresponding aqueous solutions. J. Chem. Thermodyn. 29, 1301–1310.

Urbanski, E.T., Schock, M.R., 2000. Understanding, deriving, and computing buffer capacity. J. Chem. Educ. 77, 1640–1644.

Wolff-Boenisch, D., 2011. On the buffer capacity of CO_2-charged seawater used for carbonation and subsequent mineral sequestration. Energy Proc. 4, 3738–3745.

Wolff-Boenisch, D., Gislason, S.R., Oelkers, E.H., 2004. The effect of fluoride on the dissolution rates of natural glasses at pH 4 and 25 °C. Geochim. Cosmochim. Acta 68, 4571–4582.

Wolff-Boenisch, D., Gislason, S.R., Oelkers, E.H., 2006. The effect of crystallinity on dissolution rates and CO_2 consumption capacity of silicates. Geochim. Cosmochim. Acta 70, 858–870.

Wolff-Boenisch, D., Wenau, S., Gislason, S.R., Oelkers, E.H., 2011. Dissolution of basalts and peridotite in seawater, in the presence of ligands, and CO_2: implications for mineral sequestration of carbon dioxide. Geochim. Cosmochim. Acta 75, 5510–5525.

Xu, T., Sonnenthal, E., Spycher, N., Pruess, K., 2006. TOUGHREACT—a simulation program for non-isothermal multiphase reactive geochemical transport in variably saturated geologic media: applications to geothermal injectivity and CO_2 geological sequestration. Comput. Geosci. 32, 145–165.

Xu, T., Spycher, N., Sonnenthal, E., Zhang, G., Zheng, L., Pruess, K., 2011. TOUGHREACT Version 2.0: a simulator for subsurface reactive transport under non-isothermal multiphase flow conditions. Comput. Geosci. 37, 763–774.

Yi, W.-T., Yan, C.-Y., Ma, P.-H., 2011. Kinetic study on carbonation of crude Li_2CO_3 with CO_2–water solutions in a slurry bubble column reactor. Korean J. Chem. Eng. 28, 703–709.